A versatile type VI CRISPR-based approach for targeted m^{6}A demethylation in mRNAs

Panagiotis G. Adamopoulos, Konstantina Athanasopoulou and Andreas Scorilas

Genome Res. 2026 36: 169-182 originally published online December 11, 2025
Access the most recent version at doi:10.1101/gr.280476.125

Method

A versatile type VI CRISPR-based approach for targeted m^{6}A demethylation in mRNAs

Panagiotis G. Adamopoulos,[1] Konstantina Athanasopoulou,[1] and Andreas Scorilas

Department of Biochemistry and Molecular Biology, Faculty of Biology, National and Kapodistrian University of Athens, Athens 15771, Greece

Epitranscriptomics, a rapidly evolving field mainly driven by massive parallel sequencing technologies, explores post-transcriptional RNA modifications. N^6-methyladenosine (m^{6}A) has emerged as the most prominent and dynamically regulated modification in human mRNAs, being implicated in the regulation of diverse biological processes, including spermatogenesis, heat shock response, ultraviolet-induced DNA damage response and maternal mRNA clearance. Despite the recognized significance of m^{6}A in mRNA regulation, limited studies have focused on the targeted and efficient manipulation of this modification in mRNAs. Here, we present Dem6A-Vec, an "all-in-one" plasmid vector designed for site-specific m^{6}A demethylation in human mRNAs. Dem6A-Vec integrates the expression of a catalytically inactive RfxCasl3d fused to the m^{6}A demethylase ALKBH5 and a U6-driven customizable guide RNA in a single construct, simplifying experimental workflows and enhancing targeting efficiency. Using nanopore direct RNA sequencing, we identify high-confident m^{6}A sites in HeLa cells, which serve as targets for Dem6A-Vec. We validate the targeted demethylation of m^{6}A sites in the *EEF2* and *RRAGA* genes using the established SELECT-qPCR method, confirming the impacts on mRNA stability and highlighting the tool's precision and versatility. The presented approach is implemented in multiple mRNA sites with diverse methylation stoichiometries, underscoring its adaptability to various transcriptomic contexts. This study provides a robust and scalable method for investigating the functional roles of m^{6}A modifications, offering a transformative platform for advancing epitranscriptomic research and potential therapeutic applications.

[Supplemental material is available for this article.]

Epitranscriptomics is a cutting-edge scientific field, mainly introduced to the scientific community owing to the advent of high-throughput sequencing technologies, that investigates the post-transcriptional modifications in RNA (Xiong et al. 2017). Although the existence of modified nucleosides in eukaryotic RNA molecules was confirmed decades ago, their profile, functional roles, and abundance are not yet fully disclosed (Nachtergaele and He 2017). Studies in mammalian cells have already characterized more than 170 RNA modifications, highlighting the presence of modified bases in many RNA classes, including mRNAs, long noncoding RNAs (lncRNAs), tRNAs, and rRNAs (Nombela et al. 2021). The investigation of RNA modifications necessitates the refinement of precise and sensitive detection methodologies. High-performance liquid chromatography (HPLC) coupled with mass spectrometry (MS) has emerged as the gold-standard workflow for assessing m^{6}A levels in RNA samples (Zhang et al. 2022). Although HPLC-MS guarantees accurate quantification, it is resource-intensive and time-consuming and, most importantly, fails to provide transcript-specific insights. Alternatively, antibody-based approaches, including the methylated RNA immunoprecipitation followed by sequencing (MeRIP-Seq), have garnered attention for their capability to profile m^{6}A modifications in a transcriptome-wide manner (Molinie and Giallourakis 2017; Bhattarai and Aguilo 2022). Nonetheless, these strategies present inherent limitations, such as cross-reactivity with other modified nucleotides and a deficiency in precise nucleotide resolution (McIntyre et al. 2020; Zhang et al. 2022). Recently, nanopore sequencing has emerged as a groundbreaking technology with the potential to address numerous challenges in terms of mRNA modification detection (Athanasopoulou et al. 2022; Stephenson et al. 2022). By directly analyzing RNA molecules as they pass through nanopores, this approach enables single-molecule resolution, high throughput, and the identification of modifications without requiring antibodies or chemical treatments (Leger et al. 2021). The most crucial advantage, however, is the ability to produce long sequencing reads, which facilitates the reconstruction of complete transcripts, thereby enhancing comprehension of modification context and functional implications within specific transcripts (Zheng et al. 2023).

Among all RNA modifications, N^6-methyladenosine (m^{6}A) has emerged as the most prominent and dynamically regulated modification in human mRNAs (Meyer and Jaffrey 2014). An extensive number of mRNA transcripts harbor m^{6}A modifications, each exhibiting distinct distribution patterns (Zhou et al. 2020). The incorporation of m^{6}A in mRNAs is orchestrated by methyltransferases, with the METTL3/METTL14/WTAP complex being the most widely recognized and thoroughly studied (Xu et al. 2023). Although these complexes, also known as "writers," add the methyl group to specific adenines in mRNAs, this methyl-group incorporation is reversible owing to the function of the "erasers," including FTO and/or ALKBH5 (Wang et al. 2020; Azzam et al. 2022; Yang et al. 2024). The interaction of m^{6}A "reader" proteins, such as YTHDF1–3 (Chen et al. 2023), YTHDC1/2

[1]**These authors contributed equally to this work.**
Corresponding author: padamopoulos@biol.uoa.gr
Article published online before print. Article, supplemental material, and publication date are at https://www.genome.org/cgi/doi/10.1101/gr.280476.125.

(Kretschmer et al. 2018), and IGF2BP1–3 (Ramesh-Kumar and Guil 2022), modulates mRNA splicing (Akhtar et al. 2021; Zhu et al. 2023), translation, and decay, thereby impacting protein synthesis (Shan et al. 2023). Furthermore, m^{6}A modification has been implicated in the regulation of diverse biological processes, including spermatogenesis (Tan et al. 2023), heat shock response (Zhou et al. 2015), ultraviolet-induced DNA damage response (Xiang et al. 2017), maternal mRNA clearance (Liu et al. 2022), and T cell homeostasis (Li et al. 2017). The significance of m^{6}A for cellular homeostasis has prompted many studies to focus on the development of methodologies for the efficient manipulation of this modification in mRNAs. Nevertheless, the investigation of specific RNA methylated sites is an extremely challenging task, mainly because of the lack of established methodologies. Up until recently, most of the approaches used for investigating methylation were based on manipulating the expression of RNA methyltransferase or demethylase genes, which led to broad epigenetic alterations and thus failed to provide specific information on a target site of interest.

The advent of innovative methodologies, such as those integrating CRISPR/Cas systems with RNA-processing approaches, has expedited research in this domain, furnishing novel tools for dissecting the roles of post-transcriptional modifications in gene expression dynamics and disease pathogenesis (Terns 2018; Pickar-Oliver and Gersbach 2019). The discovery of Cas13, a class 2 type VI CRISPR-Cas RNA endonuclease, has opened new avenues for targeting the dynamics of endogenous RNA transcripts and has already been used for both cleavage and subsequent degradation of RNA in various organisms, including fission yeast, plants, and mammalian cells (Abudayyeh et al. 2016; Gupta et al. 2022). Besides the identification of several Cas13 enzymes with different features, including Cas13b and Cas13d (CasRx), findings have also confirmed that specific mutations in Cas13 can produce a catalytically dead enzyme that, however, retains its RNA-binding affinity ("dead" Cas13 [dCas13]). Most importantly, fusion of dCas13 with the A-to-I RNA-editing enzymes ADAR1 or ADAR2 has been shown to perform RNA editing in a targeted manner (Cox et al. 2017). Besides ADARs, several endeavors have been dedicated to develop targeted methylation and/or demethylation approaches based on the dCas13 system, aiming to disclose the complex roles of m^{6}A in major cellular processes (Li et al. 2020; Cao et al. 2021).

Despite the progress made by the recent incorporation of fused dCas13 constructs in modern epitranscriptomics, many limitations still exist. The utilization of complex plasmid vectors expressing fused constructs along with the necessity of cotransfecting guide RNAs (gRNAs) often constitutes a significant drawback in terms of versatility and efficiency. Therefore, although the progress in developing controllable and precisely targeted RNA demethylation systems shows significant promise for exploring locus-specific RNA methylation, numerous enhancements are still necessary.

The aim of this study was to develop, optimize, and validate a versatile tool for site-specific m^{6}A demethylation in mRNAs. To this end, we present Dem6A-Vec, an in-house developed "all-in-one" plasmid vector designed to enable targeted demethylation of m^{6}A sites in human mRNAs. In contrast to previous approaches, Dem6A-Vec supports the simultaneous expression of a gRNA for the mRNA site of interest and a catalytically inactive Cas13d fused to the major m^{6}A "eraser" ALKBH5 (dCas13d-ALKBH5). The presented approach enhances flexibility and efficiency by allowing rapid targeting of diverse m^{6}A-modified mRNA transcripts through a simplified gRNA cloning workflow. Dem6A-Vec is designed to facilitate investigations into the functional roles of m^{6}A modifications at defined transcriptomic sites in human and/or other mammalian cells.

Results

Identification of the m^{6}A epitranscriptomic profile of mRNAs

Overall, a total of 3,232,027 mRNA adenine sites were tested with CHEUI for m^{6}A methylation, whereas ~9.5% (310,133 sites) of these sites had detectable methylation stoichiometry. To define high-confident m^{6}A sites with negligible false-discovery rates (FDR; approximately zero), we used CHEUI, a two-stage neural network model trained to identify and quantify m^{6}A from ionic currents derived from nanopore direct RNA sequencing (Acera Mateos et al. 2024). Consequently, most of the methylated sites were filtered out, and 3776 sites were considered as high-confident m^{6}A modifications (Fig. 1A). These m^{6}A sites were taken into consideration as candidates for the presented approach (Supplemental Table S1). Analysis highlighted that 61.55% of the identified m^{6}A sites were detected within 3′ untranslated regions (UTRs), whereas a significant proportion of 31.75% was found in the coding sequence (CDS) of mRNAs (Fig. 1B). Additionally, our findings indicate an increasing trend in the prevalence of m^{6}A sites spanning from the translation initiation codon (ATG site) to the termination codons, with the highest prevalence observed in the 3′-UTR sequence and particularly in proximity to the termination codons of mRNAs (Fig. 1C). Based on these results, we randomly selected two representative m^{6}A sites of *EEF2* and *RRAGA* genes for the development and optimization of Dem6A-Vec. These sites met stringent filtering criteria and represented well-characterized m^{6}A, making them suitable as initial targets for demethylation assays.

The consistency of the obtained results was validated by their direct comparison with records deposited in the RMBase v3.0, a comprehensive repository of RNA modifications detected and characterized by existing short-read high-throughput sequencing approaches, including m^{6}A-seq and miCLIP (Xuan et al. 2024). Direct RNA sequencing data analysis highlighted 2530 m^{6}A sites that were already deposited in RMBase v.3.0, therefore being characterized sites (Fig. 1D). Notably, the remaining 1246 detected sites represent uncharacterized m^{6}A sites that merit further investigation. Additionally, 73.6% (2782 sites) of the identified m^{6}A sites were found in the context of the 5′-DR**A**CH-3′ motifs, whereas the remaining 994 sites resided in miscellaneous non-DRACH sequences (Fig. 1E). Interestingly, 90% of the high-confident 5′-DR**A**CH-3′ sites detected in the present study are also deposited in RMBase v.3.0 and therefore represent modifications validated by antibody-based high-throughput sequencing methodologies (Fig. 1F). Motif analysis of the obtained nanopore sequencing data revealed that 5′-GG**A**CT-3′ was the most abundant methylated 5′-DR**A**CH-3′ motif, whereas noteworthy abundancies were also observed in the 5′-AG**A**CT-3′, 5′-GG**A**CC-3′, and 5′-GG**A**CA-3′ motifs (Fig. 1G).

The final part of the m^{6}A epitranscriptome analysis was the association between m^{6}A methylation and transcript abundance. For this purpose, mRNA transcripts were stratified into groups based on the m^{6}A stoichiometry levels. Our findings support that mRNA transcripts with low-stoichiometry (<0.2) m^{6}A sites demonstrate increased expression levels compared with mRNAs with highly methylated sites (Fig. 1H). However, no significant differences were observed across other stoichiometry subgroups.

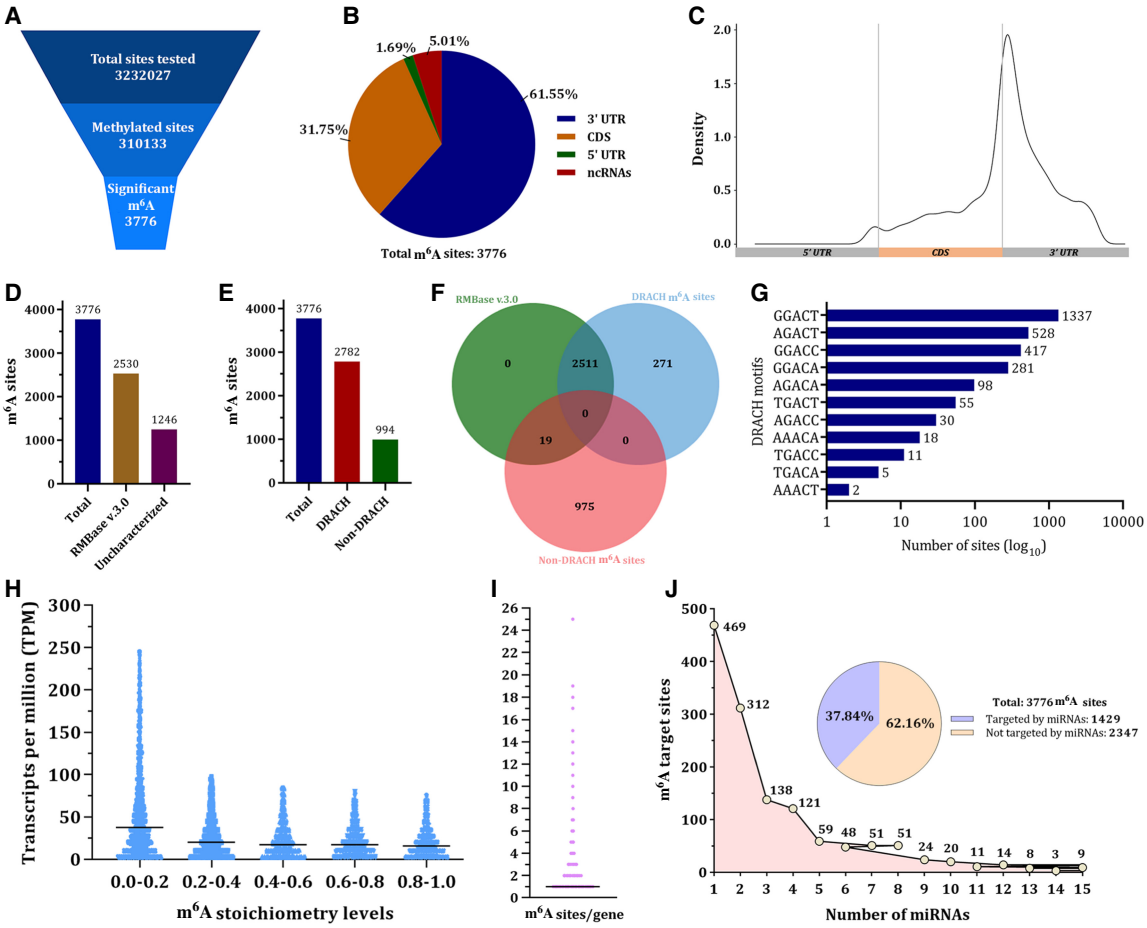

Figure 1. Descriptive analysis of the direct RNA sequencing data sets from HeLa cells. (*A*) Funnel plot exhibiting the total number of tested adenosine sites in mRNAs, the number of detected methylated sites, and the number of m^{6}A with high confidence (probability > 0.9999). (*B*) Distribution of the identified m^{6}A sites across the distinct regions of mRNAs (UTRs and CDS) as well as the proportion of m^{6}A in ncRNAs. (*C*) Density plot highlighting the relative abundance of the detected m^{6}A sites throughout the distinct regions of mRNAs (5′ UTR, CDS, and 3′ UTR). (*D*) Bar plot illustrating the number of detected m^{6}A sites that have been already deposited in RMBase v3.0, as well as the count of m^{6}A sites that are not characterized. (*E*) Bar plot indicating the total count of m^{6}A sites identified in DRACH and non-DRACH motifs of mRNAs. (*F*) Venn diagram showing the overlap between high-confident m^{6}A sites identified in this study (CHEUI probability > 0.9999) and sites deposited in RMBase v3.0. Only the 3776 high-confident sites detected by direct RNA sequencing are included in this analysis. (*G*) Total number of high-confident (probability > 0.9999) m^{6}A sites corresponding to each 5′-DR**A**CH-3′ motif on the mRNAs of HeLa cells. For visual purposes, the $\log_{10}$ value of the total count is plotted for each motif. (*H*) Scatter plots exhibiting the association of m^{6}A methylation with transcript abundance. Transcripts were stratified into groups based on the m^{6}A stoichiometry. Expression levels are shown using the transcript-per-million (TPM) method. (*I*) Number of high-confident (probability > 0.9999) m^{6}A sites per gene. A black horizontal line is used to demonstrate the median value. Only genes containing at least one m^{6}A site are demonstrated. (*J*) Proportion of high-confident m^{6}A sites (CHEUI probability > 0.9999) located within experimentally validated miRNA target regions. Binding site coordinates were obtained from the DIANA-TarBase v8 database and mapped to the transcriptome to assess overlap with identified m^{6}A sites.

Additionally, analysis showed that the m^{6}A methylome of HeLa cells is characterized by a median value of one high-confident m^{6}A site per gene (Fig. 1I). Finally, we investigated the overlap between high-confident m^{6}A sites and predicted miRNA target regions. To this end, we utilized data sets from DIANA-TarBase v8 (Karagkouni et al. 2018), a curated database of experimentally validated miRNA–mRNA interactions derived from high-throughput techniques such as PAR-CLIP. Each m^{6}A site was tested for overlap with the genomic coordinates of validated miRNA-binding sites, and the proportion of sites within miRNA target regions was quantified. Our findings support that 37.84% of the high-confident m^{6}A sites were found to reside within experimentally supported miRNA-binding regions, highlighting the potential regulatory interplay between m^{6}A modification and miRNA targeting (Fig. 1J).

Design of Dem6A-Vec for versatile targeted m^{6}A demethylation

An "all-in-one" nonviral plasmid vector, Dem6A-Vec, was designed for targeted m^{6}A demethylation (Fig. 2A). The plasmid was designed to encode the catalytically "dead" type VI-B Cas13d enzyme (mutations: R239A, H244A, R858A, and H863A) from the bacteria *Ruminococcus flavefaciens* (RfxCas13d) (Tang et al. 2022), fused to the characterized human m^{6}A demethylase ALKBH5. The fused dRfxCas13d-ALKBH5 protein was tagged with both FLAG-(DYKDDDDK) and HA-(YPYDVPDYA) in the C terminus, whereas a nuclear export signal (NES) followed by a longlinker sequence was utilized for linking the two proteins and inducing the nuclear export of the fusion protein (Fig. 2A). Furthermore, the designed plasmid confers resistance to ampicillin

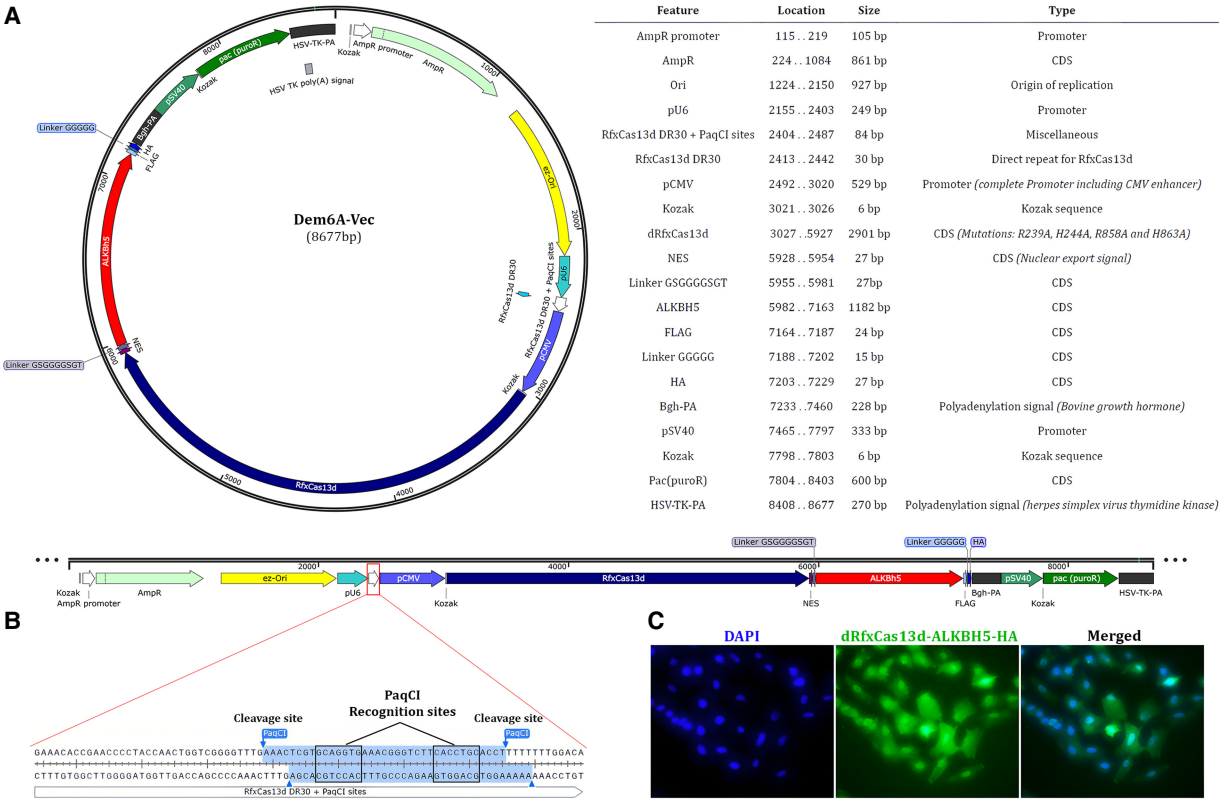

Feature	Location	Size	Type
AmpR promoter	115 . . 219	105 bp	Promoter
AmpR	224 . . 1084	861 bp	CDS
Ori	1224 . . 2150	927 bp	Origin of replication
pU6	2155 . . 2403	249 bp	Promoter
RfxCas13d DR30 + PaqCI sites	2404 . . 2487	84 bp	Miscellaneous
RfxCas13d DR30	2413 . . 2442	30 bp	Direct repeat for RfxCas13d
pCMV	2492 . . 3020	529 bp	Promoter *(complete Promoter including CMV enhancer)*
Kozak	3021 . . 3026	6 bp	Kozak sequence
dRfxCas13d	3027 . . 5927	2901 bp	CDS *(Mutations: R239A, H244A, R858A and H863A)*
NES	5928 . . 5954	27 bp	CDS *(Nuclear export signal)*
Linker GSGGGGSGT	5955 . . 5981	27bp	CDS
ALKBH5	5982 . . 7163	1182 bp	CDS
FLAG	7164 . . 7187	24 bp	CDS
Linker GGGGG	7188 . . 7202	15 bp	CDS
HA	7203 . . 7229	27 bp	CDS
Bgh-PA	7233 . . 7460	228 bp	Polyadenylation signal *(Bovine growth hormone)*
pSV40	7465 . . 7797	333 bp	Promoter
Kozak	7798 . . 7803	6 bp	Kozak sequence
Pac(puroR)	7804 . . 8403	600 bp	CDS
HSV-TK-PA	8408 . . 8677	270 bp	Polyadenylation signal *(herpes simplex virus thymidine kinase)*

Figure 2. Schematic illustration of Dem6A-Vec. (*A*) Circular map of Dem6A-Vec. The distinct features of the plasmid are shown in different colors. The location, size, and type of each feature are also exhibited. (*B*) Linear map of Dem6A-Vec. The plasmid sequence encompasses two recognition sites for the type IIS PaqCI restriction endonuclease, thus enabling the scarless cloning of any RfxCas13d-compatible gRNA of choice through golden gate cloning. (*C*) Fluorescence microscopy images highlighting the cellular localization of Dem6A-Vec.

for bacterial selection as well as resistance to puromycin for positive selection of transfected mammalian cells.

To ensure versatility in terms of targeting multiple m^{6}A sites, Dem6A-Vec enables a U6-driven expression of a Cas13d-compatible gRNA. The gRNA cloning site of Dem6A-Vec is located downstream from the 30 nt direct repeat for RfxCas13d and includes a 32 bp sequence serving as the template region for the incorporation of any gRNA sequence through the golden gate cloning method (Ran et al. 2013). Of note, the designed plasmid contains a gRNA cloning site that encompasses two cleavage sites for the type IIS PaqCI restriction endonuclease (Kennedy et al. 2023), thus enabling the scarless cloning of the gRNA sequence into the backbone sequence of Dem6A-Vec (Fig. 2B). Finally, fluorescence microscopy highlighted that after transfection, the fused dRfxCac13d-ALKBH5 construct is expressed in both the cytoplasm and nucleus of HeLa cells (Fig. 2C).

Dem6A-Vec induces the demethylation of m^{6}A sites in human mRNAs

To evaluate the efficiency of Dem6A-Vec in demethylating specific m^{6}A sites in mRNAs, we implemented the designed approach on multiple candidate m^{6}A sites that (1) were detected from direct RNA sequencing; (2) had a >0.9999 probability score from CHEUI, thus exhibiting a negligible FDR; and (3) were deposited in RMBase v.3.0 database, therefore being validated by short-read high-throughput sequencing (Supplemental Table S1). Indicatively, the present study presents detailed results of our approach on demethylating two m^{6}A sites. The first site is located within a 5′-DR**A**CH-3′ motif on the mRNA of the *EEF2* gene (GenBank transcript ID: NM_001961.4, position: 2886), whereas the second m^{6}A resides on a 5′-DR**A**CH-3′ site of the *RRAGA* mRNA (GenBank transcript ID: NM_006570.5, position: 418). For targeted demethylation, two distinct gRNA oligonucleotide duplexes were cloned into Dem6A-Vec, and assays were performed on HeLa cells. Although *EEF2* and *RRAGA* were selected as representative examples for initial optimization, primarily based on expression level and annotation quality, their selection was random among several high-confident m^{6}A sites. However, to further demonstrate the versatility of the Dem6A-Vec system, multiple m^{6}A targets with varying stoichiometries were investigated.

The demethylation efficiency of the *EEF2* and *RRAGA* target sites was evaluated in WT cells, cells transfected with Dem6A-Vec expressing a nontargeting gRNA (NT-gRNA), and cells transfected with Dem6A-Vec expressing the gRNA specific to the m^{6}A target. SELECT-qPCR assays were then conducted, targeting the m^{6}A site and a nonmethylated A nucleotide of the housekeeping *HPRT1* gene for normalization purposes. The principle of SELECT-qPCR, which efficiently amplifies nonmethylated A sites but exhibits significantly higher Ct values for m^{6}A-modified sites, was employed to assess the efficiency of demethylation.

The SELECT-qPCR results showed no significant differences in normalized m^{6}A abundance ($2^{-\Delta\Delta Ct}$ method) between WT cells and cells transfected with Dem6A-Vec expressing the NT-gRNA, indicating that Dem6A-Vec does not induce demethylation of the target site without the presence of site-specific gRNA. In

contrast, cells transfected with Dem6A-Vec expressing the gRNA targeting the m^{6}A:2886 site of *EEF2* exhibited a notable upregulation of the produced PCR product, highlighting a successful demethylation of the target (Fig. 3A). Similar results were observed for the m^{6}A:418 site of the *RRAGA* gene when the corresponding site-specific gRNA was expressed (Fig. 3B). Melt curve analysis validated the specific amplification of demethylated target sites. In contrast, WT cells and cells transfected with the NT-gRNA failed to produce PCR products, owing to the inhibitory effect of m^{6}A on the ligation step required for successful amplification (Fig. 3C).

Another important aspect of the study was to rule out the possibility that m^{6}A removal could be attributed to endogenous ALKBH5 activity rather than the expressed construct. To address this, we generated a version of Dem6A-Vec expressing a catalytically "dead" ALKBH5 variant (dALKBH5) carrying the H204A mutation (Fig. 4A). SELECT-qPCR analysis of the *EEF2* and *RRAGA* m^{6}A targets in HeLa cells transfected with the dALKBH5 construct

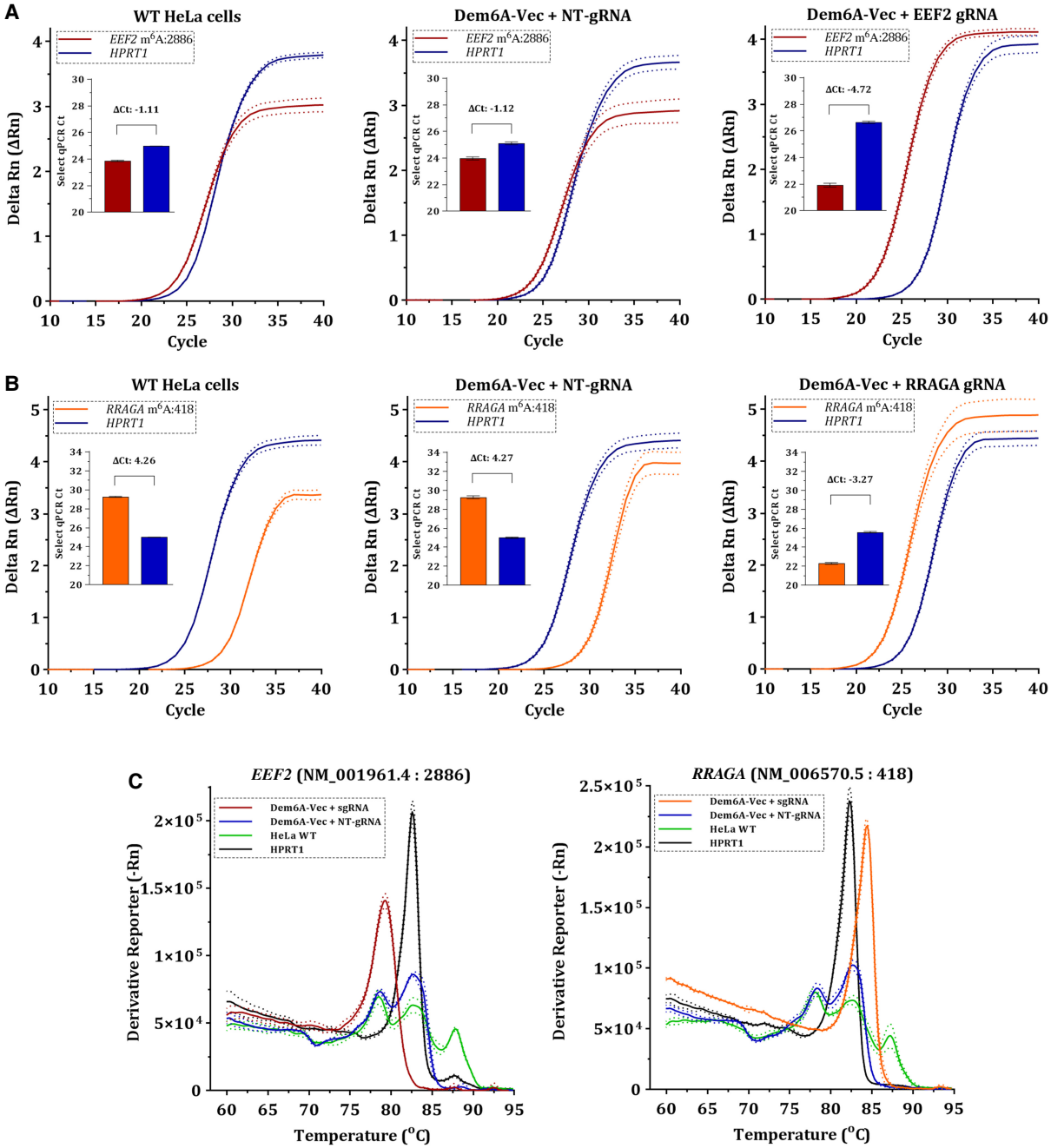

Figure 3. Demethylation impact of Dem6A-Vec at 48 h posttransfection. (*A*) Amplification plots from the implementation of SELECT-qPCR on the m^{6}A:2886 of *EEF2* and a nonmethylated site of the housekeeping *HPRT1* gene. (*B*) Amplification plots from the implementation of SELECT-qPCR on the m^{6}A:418 of *RRAGA* and a nonmethylated A site of the housekeeping *HPRT1* gene. (*C*) Melt curves generated from the SELECT-qPCR assays on the *EEF2* m^{6}A:2886 and *RRAGA* m^{6}A:418 sites.

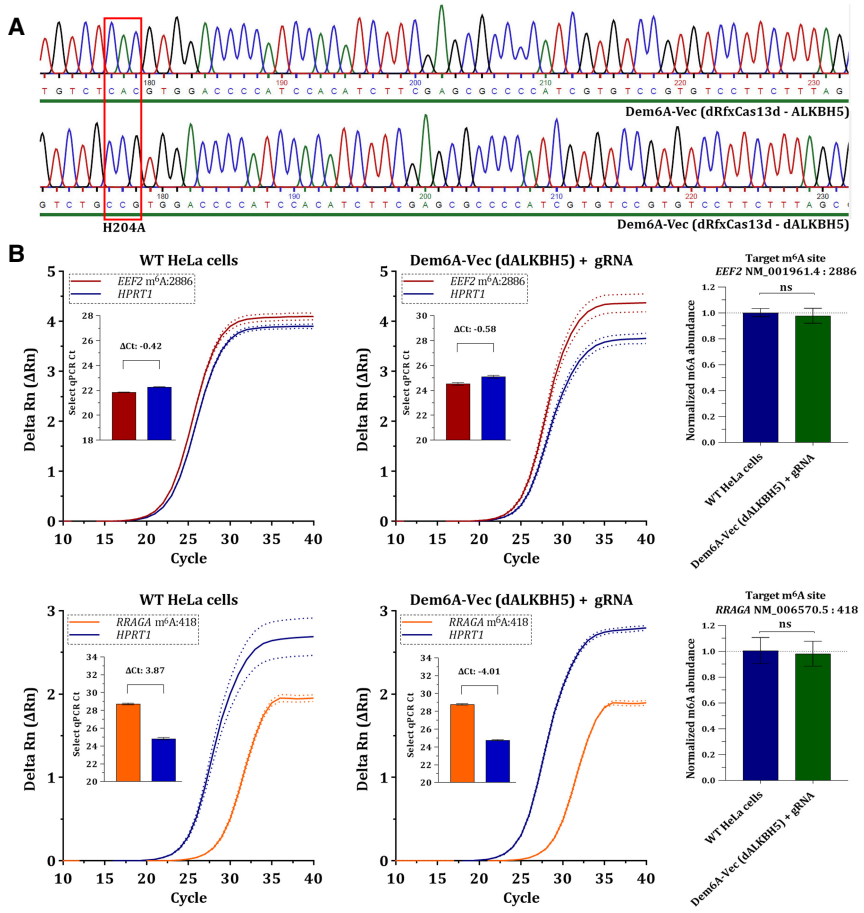

Figure 4. Investigation of the demethylation impact of Dem6A-Vec expressing a catalytically inactive ALKBH5 (dALKBH5) after site-directed mutagenesis leading to the H204A mutant enzyme. (*A*) Sanger sequencing results validating the successful generation of Dem6A-Vec expressing dALKBH5. (*B*) SELECT-qPCR results for m^{6}A:2886 of *EEF2* and m^{6}A:418 of *RRAGA* on WT HeLa cells and cells transfected with Dem6A-Vec expressing dALKBH5. The m^{6}A stoichiometry on both conditions was calculated based on the $2^{-\Delta\Delta Ct}$ methodology, using a nonmethylated A site of *HPRT1* gene as control.

revealed no significant differences compared with WT cells (Fig. 4B), confirming that demethylation depends on the enzymatic activity of the ALKBH5 in the fusion protein. Finally, to evaluate potential off-target demethylation of the designed vector across the transcriptome, we transfected cells with Dem6A-Vec expressing a NT-gRNA and performed direct RNA sequencing. Differential methylation analysis using CHEUI-diff showed no significant changes in m^{6}A stoichiometry between the HeLa WT and transfected cells, indicating that the plasmid vector itself does not alter the global m^{6}A methylome (Supplemental Fig. S1).

To further support our findings, we performed both agarose gel electrophoresis and capillary fragment analysis of SELECT-qPCR products. Based on the capillary electrophoresis in both WT and transfected cells, the ligated amplicons that correspond to successful demethylation (~75–80 bp) can be clearly discriminated from the nonligated products and adapter dimers (~40 bp) for both the *EEF2* and *RRAGA* target sites (Supplemental Fig. S2A,B). In addition, agarose electrophoresis confirms the absence of the ligated product in WT and dALKBH5-transfected cells for the *EEF2* target site (Supplemental Fig. S3). These results confirm the inability of the dALKBH5-expressing construct to perform m^{6}A editing and provide consistent findings, reinforcing the specificity of the SELECT-qPCR signal.

Dem6A-Vec induces targeted m^{6}A demethylation without affecting adjacent m^{6}A on the same mRNA

To investigate the specificity of Dem6A-Vec, we assessed whether demethylation was restricted to the target m^{6}A sites (*EEF2* m^{6}A:2886 and *RRAGA* m^{6}A:418) without affecting other m^{6}A sites within the same transcript or even completely unrelated genes. For this purpose, we investigated the potential impact of the approach on the methylated *EEF2* m^{6}A:2638 site, as well as the *RRAGA* m^{6}A:1336. Both these sites are within the same mRNAs as the previously demethylated target sites; they were detected by nanopore sequencing as high-confident sites and are deposited in RMBase v.3.0.

In cells transfected with the gRNA targeting *EEF2* m^{6}A:2886, $2^{-\Delta\Delta Ct}$ analysis showed a significant demethylation of the target site, whereas no noteworthy changes in methylation were observed at both the *EEF2* m^{6}A:2638 and *RRAGA* m^{6}A:418 sites (Fig. 5A). Similarly, in cells transfected with the gRNA targeting *RRAGA* m^{6}A:418, the target site was strongly demethylated, whereas both *EEF2* m^{6}A:2886 and *RRAGA* m^{6}A:1336 demonstrated nonsignificant methylation changes (Fig. 5B).

Demethylation of specific m^{6}A sites by Dem6A-Vec regulates mRNA stability

Because m^{6}A modifications on mRNAs are known to interfere with the stability of the transcribed product (Wang et al. 2014; He and He 2021; Chen et al. 2024), we investigated whether Dem6A-Vec can be utilized for assessing the impact of the target m^{6}A on the stability of the related mRNA. For this purpose, WT and cells transfected with Dem6A-Vec expressing the NT-gRNA, as well as with the gRNA of the target, were plated and treated with actinomycin D for 6 h. Our qPCR findings demonstrated that demethylation of both *EEF2* m^{6}A:2886 and *RRAGA* m^{6}A:418 leads to increased stability of the mRNA target in a time line of 6 h after actinomycin D treatment (Fig. 5A,B).

Dem6A-Vec enables reversible m^{6}A demethylation showcasing RNA modification plasticity

In our effort to investigate the duration of the editing effects, cells were transfected, positively selected with puromycin treatment for 24 h, and collected every 24 h for SELECT-qPCR. At every time point, qPCR was also carried out to assess the mRNA levels of *RfxCas13d*. Interestingly, $2^{-\Delta\Delta Ct}$ analysis confirmed that in both cases of the *EEF2* and *RRAGA* target sites, the highest demethylation efficiency was achieved 48 h (2 days) posttransfection (Fig.

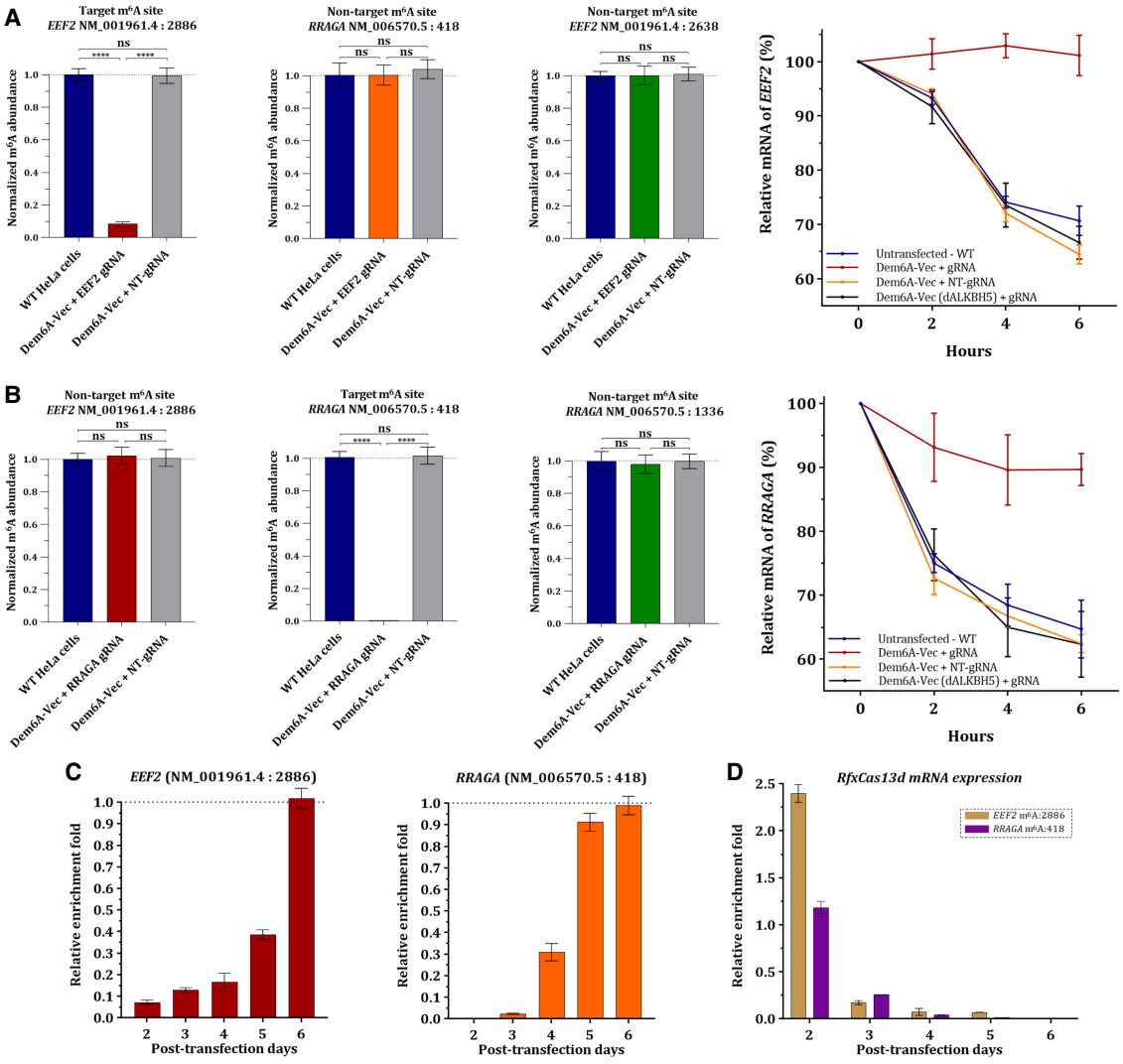

Figure 5. Assessment of the demethylation efficiency of Dem6A-Vec approach. (*A*) Targeted demethylation of the *EEF2* target site (NM_001961.4 m^{6}A:2886). Bar plots are used to demonstrate the normalized m^{6}A abundance of the target site (*EEF2* m^{6}A:2886) and two nontarget sites, *EEF2* m^{6}A:2638 and *RRAGA* m^{6}A:418. In addition, the relative expression of *EEF2* mRNA is shown under actinomycin D treatment in a time line of 6 h to evaluate the mRNA stability of the target. (*B*) Targeted demethylation of the *RRAGA* target site (NM_006570.5 m^{6}A:418). Bar plots are used to demonstrate the normalized m^{6}A abundance of the target site (*RRAGA* m^{6}A:418) and two nontarget sites, *RRAGA* m^{6}A:1336 and *EEF2* m^{6}A:2886. In addition, the relative expression of *RRAGA* mRNA is shown under actinomycin D treatment in a time line of 6 h to evaluate the mRNA stability of the target. (*C*) Graphical demonstration of the normalized m^{6}A abundance of both the *EEF2* m^{6}A:2886 and *RRAGA* m^{6}A:418 sites for a 6 day posttransfection time line. (*D*) Normalized expression levels of the *RfxCas13d* mRNA expressed by Dem6A-Vec in the transfected cells for a 6 day posttransfection time line. The human housekeeping gene *GAPDH* was used for normalization purposes.

5C). Although both targets showed substantial demethylation on day 3, partial remethylation had already initiated. As expected, higher methylation ratios were observed for days 4 and 5, with both targets being fully remethylated on day 6. Findings on the Dem6A-Vec mRNA levels point toward the same direction, because the highest plasmid expression was observed on day 2; a notable decrease was noticed on day 3; and, on day 6, plasmid expression was decreased in a hundred-fold manner (Fig. 5D).

Dem6A-Vec impacts m^{6}A sites with diverse methylation stoichiometries

To further evaluate the versatility of the presented approach, Dem6A-Vec was used to demethylate multiple m^{6}A sites with varying stoichiometries and hence provide insights into the demethylation impact on low and high methylation ratios. For this purpose, gRNAs were designed and cloned to target the following sites of several random genes: *CDC37* (NM_007065.4 m^{6}A:1145), *PSAT1* (NM_058179.4 m^{6}A:1375), *MRPL14* (NM_032111.4 m^{6}A:476), *LAMTOR2* (NM_014017.4 m^{6}A:332), *CDK2* (NM_001798.5 m^{6}A:1158), and *NAGLU* (NM_000263.4 m^{6}A:2002). All sites were detected by direct RNA sequencing as high-confident m^{6}A (Supplemental Table S1). Additionally, based on the nanopore sequencing findings, *CDC37* (NM_007065.4 m^{6}A:1145) presents a minimum of 0.05 m^{6}A stoichiometry, being the least methylated m^{6}A in HeLa transcriptome, whereas *NAGLU* (NM_000263.4 m^{6}A:2002) is a fully methylated site.

On m^{6}A sites with low methylation ratios (stoichiometry < 0.5), Dem6A-Vec demonstrated promising results in terms of

demethylation impact. In the case of the *CDC37* site, which demonstrated a minimum of 0.05 stoichiometry, only a slight decrease in m^{6}A abundancy was noticed (Fig. 6A). Despite the inherently lower baseline methylation levels, we observed noteworthy reduced m^{6}A abundance of both the *PSAT1* (m^{6}A stoichiometry: 0.16) and *MRPL14* (m^{6}A stoichiometry: 0.32) target sites (Fig. 6B, C). Notably, our results did not identify a definitive stoichiometry threshold under which demethylation was entirely ineffective.

At m^{6}A sites exhibiting high stoichiometry (>0.5), our approach induced a robust and consistent demethylation effect. Based on the $2^{-\Delta\Delta Ct}$ method, the target sites of *LAMTOR2* (NM_014017.4 m^{6}A:332) and *CDK2* (NM_001798.5 m^{6}A:1158) were significantly demethylated (Fig. 7A,B). Similarly, on the fully methylated site of *NAGLU* (NM_000263.4 m^{6}A:2002), Dem6A-Vec exhibited a significant reduction in methylation levels (Fig. 7C). Notably, removal of the each m^{6}A target was also confirmed by the fact that successful generation of qPCR amplicon in the melt curve analysis was clearly observed only in the edited cells. It should be mentioned that because SYBR Green methodology was used for qPCR detection, minor signals from dimers can occasionally appear and are highly dependent on the specific primers used for the site of interest (Fig. 7B). Collectively, these findings emphasize the adaptability of Dem6A-Vec as a demethylation tool capable of targeting m^{6}A sites irrespective of their initial stoichiometry. This versatility highlights its utility for investigating the m^{6}A functionality in mRNAs with varying methylation dynamics.

Discussion

The field of epitranscriptomics has garnered considerable attention owing to its potential to unveil the intricate regulatory roles of RNA modifications. Among these modifications, m^{6}A has emerged as the most abundant and dynamically regulated in eukaryotic mRNAs (Liu et al. 2020). Studies have demonstrated that m^{6}A influences various mRNA features, including stability, splicing, export, translation, and degradation (Roundtree et al. 2017; Zaccara and Jaffrey 2020). The introduction of CRISPR/Cas13d has revolutionized epitranscriptomics by providing a robust tool for RNA processing and precise manipulation (Wessels et al. 2020). A significant advancement in this field is the development of fused constructs that integrate catalytically inactive Cas13d with effector domains, such as methyltransferases or demethylases (Konermann et al. 2018; Cao et al. 2021). This enables the specific manipulation rather than degradation of the RNA target. Although this targeted approach holds great promise for advancing research

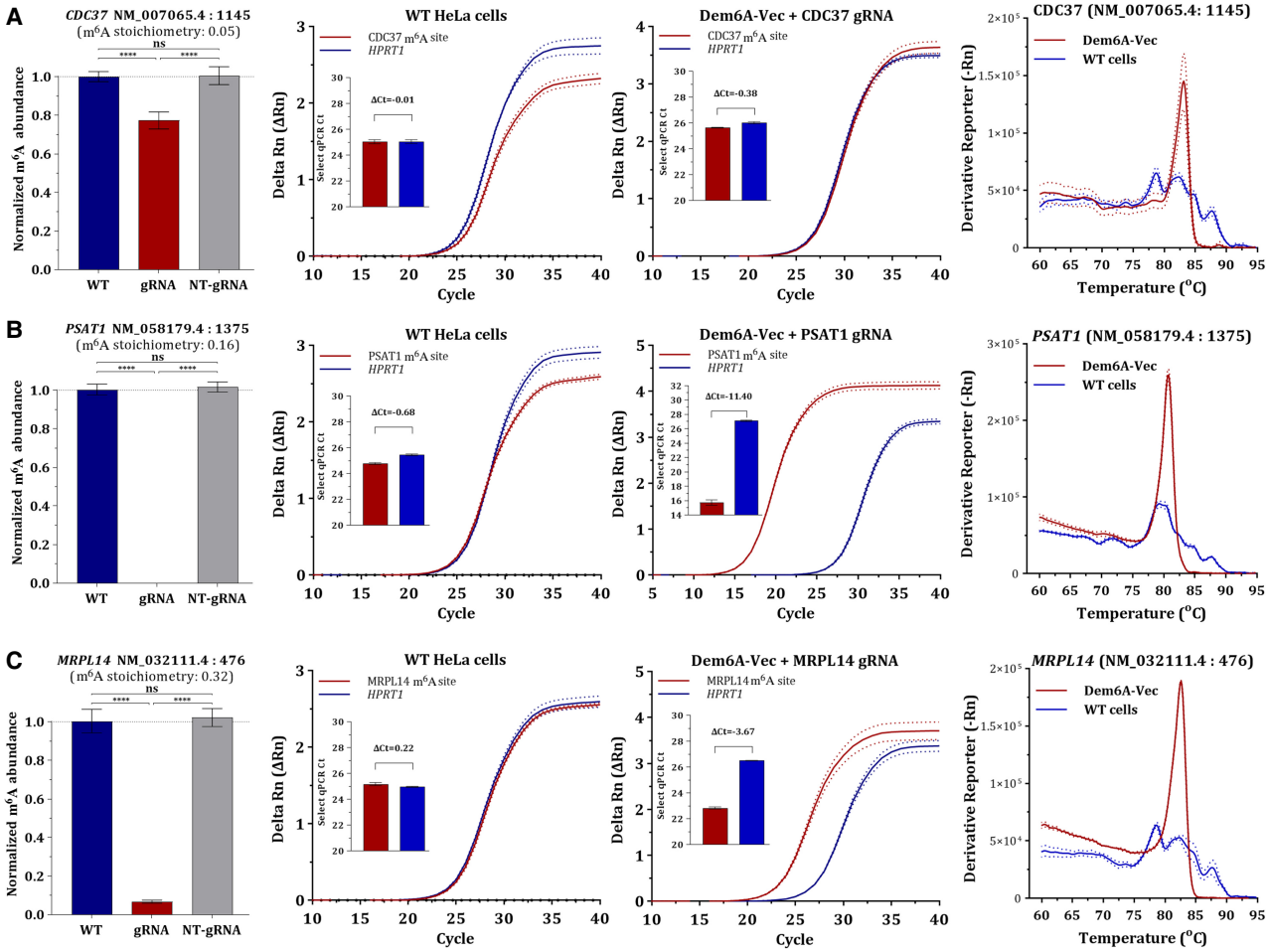

Figure 6. Evaluation of the presented targeted demethylation approach on high-confident m^{6}A targets with <0.5 methylation stoichiometries. SELECT-qPCR data and normalized m^{6}A abundance are shown for *CDC37* (NM_007065.4 m^{6}A:1145; *A*), *PSAT1* (NM_058179.4 m^{6}A:1375; *B*), and *MRPL14* (NM_032111.4 m^{6}A:476; *C*) at 48 h posttransfection with Dem6A-Vec expressing the target gRNAs.

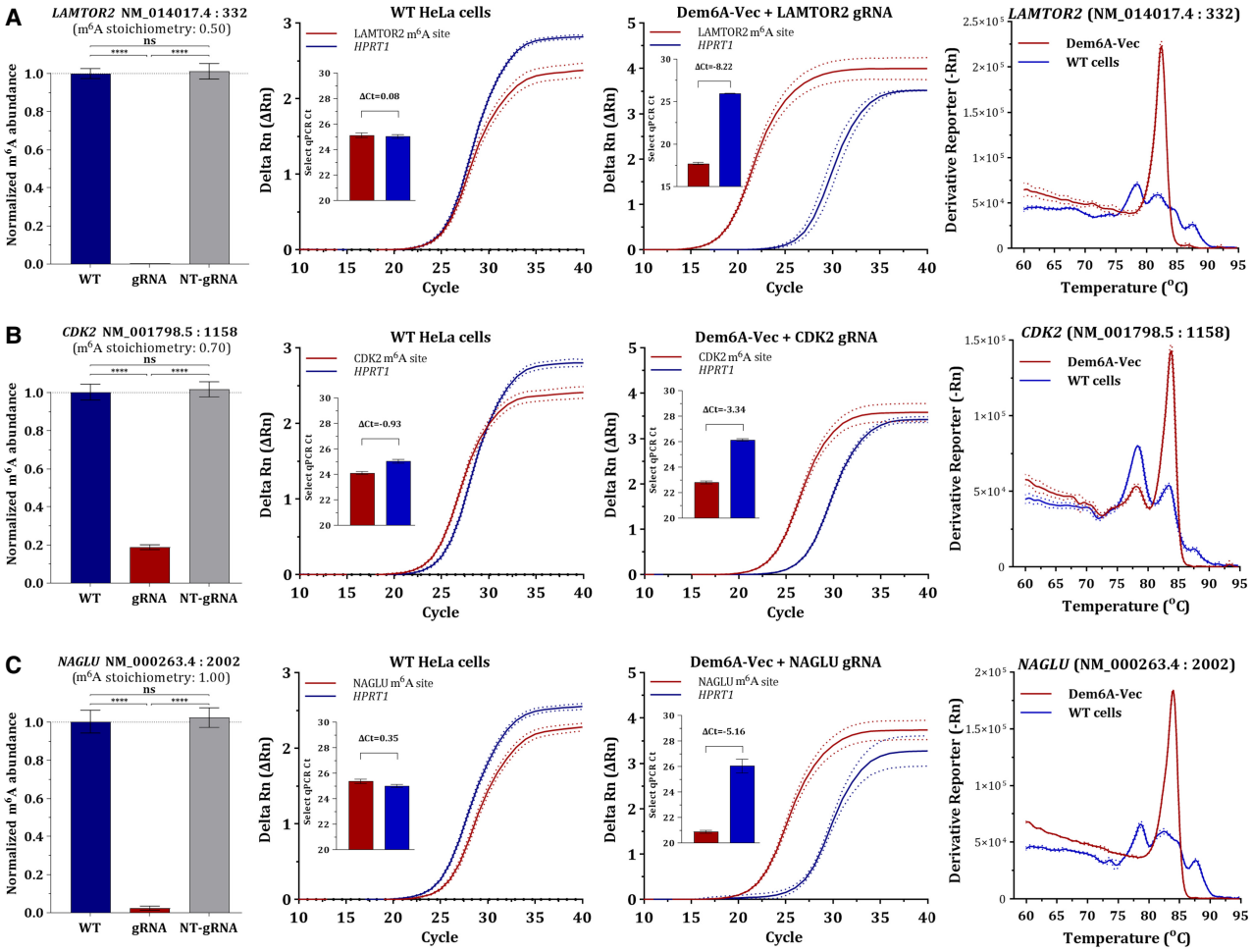

Figure 7. Evaluation of the presented targeted demethylation approach on high-confident m^{6}A targets with >0.5 methylation stoichiometries. SELECT-qPCR data and normalized m^{6}A abundance are shown for *LAMTOR2* (NM_014017.4 m^{6}A:332; *A*), *CDK2* (NM_001798.5 m^{6}A:1158; *B*), and *NAGLU* (NM_000263.4 m^{6}A:2002; *C*) at 48 h posttransfection with Dem6A-Vec expressing the target gRNAs.

and developing novel therapeutic applications, the current number of studies utilizing tools for precise RNA manipulation is limited.

In the present study, we introduce Dem6A-Vec, an in-house developed plasmid vector designed for targeted m^{6}A demethylation in human mRNAs. One primary advantage of Dem6A-Vec is its versatile "all-in-one" plasmid design, integrating the expression of catalytically inactive RfxCas13d fused with the major human m^{6}A demethylase ALKBH5, as well as the U6-driven expression of any gRNA compatible with CasRx (Fig. 2A). Among the identified and studied Cas13 effector proteins, including AdmCas13d, EsCas13d, and LwaCas13a, Dem6A-Vec was designed to express RfxCas13d because this effector protein has been shown to demonstrate the most robust results in terms of targeted mRNA engineering (Konermann et al. 2018).

The design of all gRNAs utilized in the present study were based on the already identified optimal gRNA features for RfxCas13d (Xia et al. 2021). Given that RfxCas13d can, in principle, target any RNA sequence with the appropriate gRNA design, all high-confident m^{6}A sites identified in our direct RNA sequencing data set could theoretically serve as Dem6A-Vec targets. The only technical constraint arises in cases in which a gRNA sequence contains the recognition site for the PaqCI restriction enzyme used in golden gate cloning. However, because PaqCI recognizes a 7 nt motif (5′-CACCTGC-3′), the likelihood of this occurring is extremely low. In such rare cases, alternative gRNA designs can resolve the issue, preserving the system's broad applicability. Another significant aspect of the gRNA design for the presented approach is the potential off-target activity. To assess any potential off-target activity within the target mRNA, we evaluated the methylation status of two additional m^{6}A sites, *EEF2* m^{6}A:2638 and *RRAGA* m^{6}A:1336, which are located within the same mRNAs as our target sites but were not targeted by the expressed gRNAs. SELECT-qPCR analysis revealed no significant changes in methylation at these nontarget sites. Although these results are encouraging, it is highly anticipated that any potential off-target effects would primarily depend on the sequence complementarity and specificity of the designed gRNA. Thus, transcriptome-wide off-target analysis is highly recommended for each gRNA prior to any RNA editing experiment.

In addition to HeLa cells, we sought to explore the broader applicability of Dem6A-Vec in cell types that are typically more resistant to transfection. Thus, we tested the plasmid vector in BJ and NIH/3T3 fibroblast cells and confirmed robust expression of the

construct, using fluorescence microscopy. The observed results suggest that, despite the inherent challenges in transfecting primary-like and fibroblast cell lines, Dem6A-Vec can still achieve efficient delivery and expression (Supplemental Material). This expands the potential use of our tool to a wider range of biological systems and experimental contexts.

The presented approach has a differentiated design compared with previously published methods that require separate plasmids for the Cas13-ALKBH5 fusion construct and the gRNAs, necessitating multiple transfections or cotransfections and increasing the complexity of the experimental setup (Rau et al. 2019; Cao et al. 2021). The transfection of separate plasmids for the Cas-ALKBH5 fusion protein and gRNAs not only complicates the experimental workflow but also introduces variability in transfection efficiency, which may lead to inconsistent expression levels of the required components and thus may affect the efficiency and specificity of the targeted demethylation process. By incorporating these components into a single plasmid, Dem6A-Vec simplifies the process of targeted RNA editing. This "all-in-one" design ensures codelivery and coexpression of both the dRfxCas13d-ALKBH5 fusion protein and the gRNA within the same cells, thereby minimizing variability introduced by cotransfection of multiple plasmids. Although expression levels are influenced by factors such as promoter strength, the use of a single vector ensures that both components are present in the same cellular context, which is essential for the assembly and activity of the RNA-processing complex. Additionally, the unified plasmid system reduces the total amount of transfected DNA, which may help limit cytotoxicity and enhance transfection efficiency and reproducibility.

Besides enhancing the reproducibility and scalability of experiments, the use of a single plasmid vector opens new possibilities for combinatorial studies, enabling the rapid investigation of multiple m^{6}A sites by simply altering the gRNA sequence within the plasmid. Undoubtably, this flexibility has the potential to accelerate the investigation of the functional roles of specific m^{6}A modifications across various mRNA targets and biological contexts. To obtain candidate m^{6}A targets for validating our approach, we implemented direct RNA sequencing on HeLa cells and performed m^{6}A calling with CHEUI (Acera Mateos et al. 2024). However, we took into consideration only the m^{6}A sites that demonstrated negligible FDR values (methylation probability > 0.9999) and were also deposited in the RMBase v3.0 database (Xuan et al. 2024), therefore being validated with short-read high-throughput sequencing (Supplemental Table S1).

In the present study, we demonstrated the targeted demethylation of two characterized m^{6}A sites on the *EEF2* and *RRAGA* mRNAs using Dem6A-Vec (Fig. 3A,B), whereas m^{6}A targets of multiple genes (*CDC37*, *PSAT1*, *MRPL14*, *LAMTOR2*, *CDK2*, and *NAGLU*) with diverse methylation stoichiometries were used for validation of the approach. Demethylation efficiency for each investigated target was assessed based on the $2^{-\Delta\Delta Ct}$ method from the SELECT-qPCR results. For demethylation assessment of *EEF2* and *RRAGA* m^{6}A sites in both WT and transfected HeLa cells, a targeted GLORI approach was also performed as previously described in a recent study, using reverse transcription of treated mRNA followed by nested PCR (Supplemental Fig. S4A,B; Sun et al. 2025). Although demethylation is verified by both approaches, differentiations in stoichiometry are expected mainly owing to the random nested PCR-based amplification resulting from the heavy mRNA fragmentation induced by the GLORI treatment as well as the limited quantification accuracy that SELECT-qPCR may exhibit. Specifically, for *EEF2* and *RRAGA* m^{6}A targets, SELECT-qPCR analysis supported that demethylation impact is fully reversible in a time line of 6 days posttransfection (Fig. 5C). Finally, our findings demonstrated that Dem6A-Vec induces targeted demethylation of m^{6}A in mRNAs, influencing their stability, and therefore represents a robust and versatile tool for mRNA epitranscriptomics.

Another key feature of the presented approach is the choice of the restriction enzyme used for golden gate cloning of gRNAs into Dem6A-Vec. The developed approach involves the utilization of the restriction endonuclease PaqCI, which is a type IIS restriction enzyme recognized for its robustness and precision, especially in applications like golden gate assembly (Kennedy et al. 2023). PaqCI recognizes a unique 7 nt palindromic sequence, a feature that distinguishes it from many other restriction enzymes that typically recognize shorter sequences (Marillonnet and Werner 2019; Tasnim et al. 2023). Hence, the incorporation of two PaqCI cleavage sites into Dem6A-Vec for gRNA cloning is particularly beneficial in terms of modifying the plasmid vector and using different fused constructs with other effector proteins, because this longer recognition sequence reduces the chances of additional cuts in the effector protein. Consequently, although Dem6A-Vec is presented as a m^{6}A demethylation vector, it is designed in a way that is adjustable for fusing Cas13d with other effector proteins that include methyltransferases (Wilson et al. 2020), demethylases (Li et al. 2020), or even modification-specific reader proteins (Rauch et al. 2018), enabling a wide variety of applications in epitranscriptomic research (Cox et al. 2017; Shi and Wu 2024). Specifically, the primary m^{6}A eraser ALKBH5 that was utilized in this study can be substituted with other "writers," "erasers," or even "readers." Indicatively, Dem6A-Vec could be used after the substitution of ALKBH5 with any member of the human ALKBH family because no restriction site is recognized by PaqCI. This adaptability allows researchers to expand the utility of Dem6A-Vec to investigate a wide range of RNA modifications beyond m^{6}A, such as m5C (Zhang et al. 2024), pseudouridine, and inosine (Wang et al. 2023). Hence, by enabling the incorporation of various effectors, Dem6A-Vec provides a powerful tool for dissecting the functional roles of different RNA modifications in transcript stability, translation, and cellular homeostasis. This flexibility underscores its potential to drive discoveries across diverse fields of epitranscriptomics and RNA biology, offering opportunities to better understand the regulatory networks mediated by RNA modifications and their implications in health and disease.

The subcellular localization of Cas13d fusion proteins is increasingly recognized as a critical factor influencing RNA-processing efficiency. Although CasRx is generally cytoplasmic, its localization can shift depending on the fusion partner and the nuclear retention of crRNAs. Recent studies have demonstrated that adding an NES signal can enhance cytoplasmic activity by facilitating the export of Cas13d–crRNA complexes (Gruber et al. 2024). Based on this rationale, we incorporated a C-terminal NES into our construct to promote access to cytoplasmic mRNAs. Fluorescence microscopy confirmed that the expressed dCasRx-ALKBH5 fusion protein localizes to the cytoplasm but is also detectable in the nucleus (Fig. 2C). As various localization strategies continue to be explored, Dem6A-Vec has been designed to allow substitution of the NES with alternative signals, enabling further adaptation in future applications.

In summary, Dem6A-Vec constitutes an alternative and versatile approach for mRNA epitranscriptomic research by addressing the existing drawbacks of previous methods and providing a comprehensive and efficient approach for targeted m^{6}A demethylation.

Its integration of both the demethylase and gRNA components into a single plasmid not only simplifies the experimental process but also enhances the precision, reproducibility, and scalability of epitranscriptomic studies. By providing a versatile and efficient tool for targeted m^{6}A demethylation, our study lays the groundwork for a deeper exploration of the functional roles of m^{6}A modifications in gene expression and disease. The insights gained from this research have the potential to drive the development of novel therapeutic strategies targeting RNA modifications.

Methods

Cell culture

HeLa (cervical carcinoma) cells were propagated in Eagle's minimum essential medium (2 mM L-glutamine, 1 mM sodium pyruvate, 1.5 g/L NaHCO3, w: NEAA, w: EBSS), supplemented with 10% fetal bovine serum (FBS; Gibco/Life Technologies) and 1% penicillin/streptomycin (Biosera), at 37°C and 5% CO_2. Dissociation of cells was performed upon 80%–90% confluency with trypsin–EDTA solution (Biowest) with a passaging ratio of 1:4.

Total RNA extraction and mRNA enrichment

The TRIzol reagent (Ambion, Thermo Fisher Scientific) was used for the total RNA isolation from HeLa cells. In the next step, mRNA enrichment was carried out with the Magnosphere UltraPure mRNA purification kit (Takara Bio), following the guidelines of the manufacturer. The quality and concentration of total and poly(A)+ RNA samples were evaluated by capillary electrophoresis on the Agilent 2100 bioanalyzer, using the RNA 6000 Pico kit (Agilent Technologies).

Direct mRNA sequencing

An initial amount of 500 ng mRNA sample was used for the library construction protocol for nanopore sequencing. For this purpose, the direct RNA sequencing kit (SQK-RNA002, Oxford Nanopore Technologies [ONT]) was used, based on the manufacturer's protocol. Briefly, the annealing and ligation of the RT adapter in the 3′ poly(A) tails of mRNAs were carried out by incubating each mRNA sample for 10 min at room temperature, using a T4 DNA ligase (New England Biolabs). Reverse transcription was performed in a 40 µL reaction volume on a Veriti 96-well fast thermal cycler (Applied Biosystems). The produced cDNA sample was purified with 1.8× Agencourt RNAClean XP beads (Beckman Coulter). The RNA adapter (RMX) was then ligated to the cDNAs in a 10 min room temperature incubation with T4 DNA ligase in a 40 µL reaction volume, and then a second purification with 0.4× Agencourt RNAClean XP beads was carried out. The final library was loaded on a FLO-MIN106D flow cell with R9.4.1 chemistry, and the sequencing run was performed on a MinION Mk1C sequencer (ONT), producing 1.22 million reads.

m^{6}A epitranscriptome analysis

Raw sequencing data were basecalled with Guppy v.6.2.1 using the RNA model rna_r9.4.1_70bps_hac with the default read Q-score filtering. Only sequencing reads that passed the quality filtering were further processed. Basecalled sequenced reads were aligned to the reference human transcriptome (NCBI RefSeq assembly: GCF_000001405.40) using minimap2 (version 2.22) (Li 2018). Additionally, IsoQuant was employed for expression analysis and transcript quantification (Prjibelski et al. 2023). Indexing and event aligning of the basecalled reads to the reference transcriptome were conducted with nanopolish v. 0.14. Detection of m^{6}A sites was carried out using the default pipeline parameters of CHEUI, a two-stage neural network software capable of identifying and quantifying m^{6}A sites in nanopore RNA sequencing data sets (Acera Mateos et al. 2024). Transcriptomic sites covered with at least eight sequencing reads were taken into consideration for m^{6}A calling. All identified m^{6}A sites were associated with a prediction probability score, ranging from zero to one. The called m^{6}A sites exhibiting a prediction probability > 0.9999 were considered as high-confident because they are characterized by a negligible FDR. All high-confident m^{6}A sites detected in HeLa cells were tested on whether they were already deposited in RMBase v.3.0 (Xuan et al. 2024) and hence represented validated m^{6}A sites with antibody based high-throughput sequencing approaches. Only high-confident m^{6}A sites that were also deposited in RMBase v.3.0 were taken into consideration as putative m^{6}A targets for the present methodology.

Dem6A-Vec engineering, design of gRNAs, and golden gate cloning

Engineering and delivery of Dem6A-Vec was carried out by Polyplus. Targeted demethylation of any m^{6}A site through Dem6A-Vec requires the design of two single-stranded oligonucleotides (gRNA top and gRNA bottom). The gRNA top sequence should be complementary to the mRNA target sequence. Because the optimal gRNA design has already been elucidated for the Cas13d expressed by Dem6A-Vec (Wessels et al. 2020; Xia et al. 2021), all gRNA sequences were designed following the existing literature. In this study, gRNA top and gRNA bottom oligonucleotides were designed to target m^{6}A sites of *EEF2* and *RRAGA* genes, as well as several mRNA sites demonstrating differential methylation stoichiometries (Supplemental Table S2).

Annealing of the two oligos was carried out in reaction volumes of 10 µL containing 6 µL RNase-free H_2O, 1 µL of each gRNA oligo (100 µM), 1 µL of 10× T4 ligation buffer (New England Biolabs), and 1 µL (10U) of T4 polynucleotide kinase (New England Biolabs). The reaction mixture was incubated for 30 min at 37°C, followed by 5 min at 95°C and a ramp down step to 25°C at 5°C/min in a Veriti 96-well fast thermal cycler (Applied Biosystems). The phosphorylated annealed oligos were diluted 1:200 in H_2O, and the subsequent cloning reaction was carried out in 20 µL containing 100 ng of the designed plasmid, 2 µL of the diluted annealed oligos, 2 µL of 10× T4 ligation buffer (New England Biolabs), 1 µL (10U) of PaqCI (New England Biolabs), 0.5 µL of PaqCI activator (New England Biolabs), 1 µL of T4 DNA ligase (New England Biolabs), and H_2O. The 20 µL cloning reaction was incubated for 10 cycles: 10 min at 37°C and 5 min at 16°C. In the last step, the ligation reaction was treated with exonuclease V (RecBCD) for the removal of any liner DNA fragments. For this purpose, the total ligation reaction volume of 20 µL was mixed with 5 µL 10× NEB buffer 4, 5 µL of ATP (10 mM), 1 µL (10U) of RecBCD (New England Biolabs), and 19 µL H_2O to a final volume of 50 µL. Incubation was carried out for 60 min at 37°C, followed by a heat inactivation step for 30 min at 70°C. Finally, 5 µL of the RecBCD-treated reaction was mixed with 100 µL NZY5α competent cells (NZYtech) for bacterial transformation, based on the protocol of the manufacturer. The successful gRNA cloning to Dem6A-Vec was validated with Sanger sequencing using the primer 5′-GAGGGCCTATTTCCCATGATTCC-3′, which anneals to the U6 promoter sequence (Supplemental Material).

Site-directed mutagenesis

The Q5 site-directed mutagenesis kit was used to generate a Dem6A-Vec version expressing the H204A-mutated and thus

catalytically inactive ALKBH5 (Zheng et al. 2013). Briefly, the first step included an exponential PCR-based amplification step using specifically designed forward (5′-CATCGTGTCTGCCGTGGACC CCATCCACATCTTC-3′) and reverse (5′-CAGCCGCCGGGCTGG TAG-3′) primers, which enabled the incorporation of the desired nucleotide substitutions. Then, the generated PCR product was subjected to kinase, ligase, and DpnI (KLD) treatment, following the protocol of the manufacturer. The treated PCR product was used for bacterial transformation, whereas validation of the successful targeted mutagenesis was performed with Sanger sequencing.

Plasmid transfection

HeLa cells were plated in six-well cell culture plates. Cells were plated 24 h prior to transfection in 3 mL complete medium per well. For each well, transfection was carried out using Opti-MEM I reduced serum medium (Gibco/Life Technologies), 4 µL Lipofectamine 3000 (Invitrogen, Thermo Fisher Scientific), 2.5 µg of plasmid DNA, and 4 µL of P3000 reagent. At 24 h after transfection, cells were treated with 2 µg/mL puromycin for the positive selection of the successfully transfected cells. The transfected cells were appropriately harvested, and total RNA extraction was performed for downstream analysis.

To evaluate the *RfxCas13d* mRNA expression in the transfected cells, total RNA was treated with DNase I (New England Biolabs), and then, reverse transcription was performed using random hexamers (Thermo Fisher Scientific). The generated cDNA was amplified with a qPCR-based assay using gene-specific primers for *RfxCas13d* (Supplemental Table S3), whereas the housekeeping gene *GAPDH* was used for normalization.

Fluorescence microscopy

To investigate the plasmid localization through fluorescence microscopy, an immunofluorescence application solutions kit, HA-Tag (C29F4), rabbit mAb and anti-rabbit IgG (H+L), F(ab′)2 fragment (Alexa Fluor 488 Conjugate) were purchased from Cell Signaling Technology. At 24 h postselection, HeLa cells were fixed with 4% formaldehyde for 15 min at room temperature and rinsed three times with 1× PBS for 5 min each. For immunostaining, cells were blocked using blocking buffer under shaking conditions for 60 min. Cells were then incubated with HA-tag (C29F4) rabbit mAb (1:800 dilution, Cell Signaling Technology 3724S) in antibody dilution buffer overnight at 4°C. After rinsing three times with 1× PBS, cells were incubated with fluorochrome-conjugated secondary antibody, anti-rabbit IgG (H+L), and F(ab′)2 fragment (Alexa Fluor 488 Conjugate, Cell Signaling Technology 4412S) diluted 1:600 in antibody dilution buffer for 2 h at room temperature in the dark. Finally, cells were rinsed with 1× PBS and stained with DAPI using ProLong gold antifade reagent with DAPI (Thermo Fisher Scientific P36935). Fluorescence images were captured using a Carl Zeiss Axio Vert.A1 microscope.

To evaluate the applicability of Dem6A-Vec in cell lines with lower transfection efficiency, BJ (human fibroblast) and NIH/3T3 (mouse embryonic fibroblast) cells were transfected using Lipofectamine 3000, following the same conditions as for HeLa cells. At 24 h postselection, cells were subjected to immunofluorescence staining, using anti-HA and/or anti-FLAG antibodies as described above, to confirm successful expression and localization of the Dem6A-Vec construct (Supplemental Material).

Single-base elongation and ligation-based qPCR amplification method

The already established elongation and ligation-based qPCR amplification method (SELECT-qPCR) was implemented to assess the efficiency of the presented targeted transcriptome engineering approach (Xiao et al. 2018). Based on this method, we designed two synthetic DNA oligos (UP and DOWN primers) containing adapter sequences that were designed to trap the target the m^6A sites of the *EEF2* and *RRAGA* genes (Supplemental Table S4). After ligation, site-specific amplification was performed using qPCR based on the SYBR Green method. Relative m^6A abundance was calculated using the $2^{-\Delta\Delta Ct}$ method, in which ΔCt was defined as the difference between the Ct value of the target site and that of the nonmethylated internal control of *HPRT1*, and ΔΔCt was the difference between the ΔCt of each sample and that of HeLa WT cells used as the reference condition. Relative m^6A levels were then expressed as $2^{-\Delta\Delta Ct}$, enabling the evaluation of site-specific demethylation efficiency across conditions.

The initial mixtures included 1500 ng of total RNA as template, 40 nM UP primer, 40 nM DOWN primer, and 5 µM dNTPs in a total volume of 17 µL in 1× CutSmart buffer (New England Biolabs). The mixture was incubated in a hot-lid Veriti 96-well fast thermal cycler (Applied Biosystems) with the following thermal conditions: 1 min at 90°C, 1 min at 80°C, 1 min at 70°C, 1 min at 60°C, and 1 min at 50°C and then 6 min at 40°C. The final reaction mixtures were completed by adding 3 µL of 0.02 U Bst 2.0 DNA polymerase (New England Biolabs), 0.5 U SplintR ligase (New England Biolabs), and 10 nmol ATP and were incubated for 20 min at 40°C. The reaction was terminated by heat inactivation for 20 min at 80°C and stored at 4°C. For the amplification of the m^6A regions of interest, qPCR assays based on the SYBR Green method were performed in a 96 fast well block QuantStudio 5 real-time PCR system (Thermo Fisher Scientific), using primers designed to anneal at the adapter sequences of UP and DOWN DNA oligos (Supplemental Table S4). Briefly, cycling conditions of qPCR reactions were as follows: 5 min at 95°C, (10 sec at 95°C; 15 sec at 60°C) repeated for 40 cycles, 15 sec at 95°C, 1 min at 60°C, 15 sec at 95°C (collecting fluorescence at a ramping rate of 0.05°C/sec), and, finally, a hold at 4°C. The qPCR data were analyzed using QuantStudio design and analysis software.

mRNA stability assay

HeLa cells were plated in 24-well plates and transfected with 0.5 µg plasmid expressing the target gRNAs and the NT-gRNA. Cells were selected with 2 µg/mL puromycin, added 24 h posttransfection. Puromycin treatment was removed after 24 h. In the next step, both transfected and WT cells were treated with actinomycin D (Gibco, Thermo Fisher Scientific) at 5 µg/mL for 0, 2, 4, and 6 h. Cells were collected and total RNA was extracted and reverse-transcribed as previously described. The first-strand cDNAs were used as templates for qPCR using gene-specific primers (Supplemental Table S3), whereas the housekeeping gene *GAPDH* was used for normalization.

Statistical analysis

Results are demonstrated as mean ± SD from three independent experiments. Data were analyzed by a two-tailed unpaired Student's *t*-test between two groups. Statistical analysis was carried out using GraphPad Prism 9. All statistical tests were two-sided ($^*P < 0.05$, $^{**}P < 0.01$, $^{***}P < 0.001$, $^{****}P < 0.0001$, ns: no significance).

Data access

The sequencing data generated in this study have been submitted to the NCBI BioProject database (https://www.ncbi.nlm.nih.gov/bioproject/) under accession number PRJNA1256807.

Competing interest statement

The authors declare no competing interests.

Acknowledgments

This research project was supported by the Hellenic Foundation for Research and Innovation (H.F.R.I.) under the "3rd Call for H.F.R.I. Research Projects to support Post-Doctoral Researchers" (project no. 07261).

Author contributions: Conceptualization, supervision, methodology, bioinformatics analysis, and writing of the original draft preparation were by P.G.A. Methodology, bioinformatics analysis, data curation, and writing of the original draft preparation were by K.A. A.S. reviewed and edited the manuscript.

References

Abudayyeh OO, Gootenberg JS, Konermann S, Joung J, Slaymaker IM, Cox DB, Shmakov S, Makarova KS, Semenova E, Minakhin L, et al. 2016. C2c2 is a single-component programmable RNA-guided RNA-targeting CRISPR effector. *Science* **353:** aaf5573. doi:10.1126/science.aaf5573

Acera Mateos P, Sethi AJ, Ravindran A, Srivastava A, Woodward K, Mahmud S, Kanchi M, Guarnacci M, Xu J, Yuen WS, et al. 2024. Prediction of m6A and m5C at single-molecule resolution reveals a transcriptome-wide co-occurrence of RNA modifications. *Nat Commun* **15:** 3899. doi:10.1038/s41467-024-47953-7

Akhtar J, Lugoboni M, Junion G. 2021. m^{6}A RNA modification in transcription regulation. *Transcription* **12:** 266–276. doi:10.1080/21541264.2022.2057177

Athanasopoulou K, Boti MA, Adamopoulos PG, Skourou PC, Scorilas A. 2022. Third-generation sequencing: the spearhead towards the radical transformation of modern genomics. *Life (Basel)* **12:** 30. doi:10.3390/life12010030

Azzam SK, Alsafar H, Sajini AA. 2022. FTO m6A demethylase in obesity and cancer: implications and underlying molecular mechanisms. *Int J Mol Sci* **23:** 3800. doi:10.3390/ijms23073800

Bhattarai DP, Aguilo F. 2022. m^{6}A RNA immunoprecipitation followed by high-throughput sequencing to map N^6-methyladenosine. *Methods Mol Biol* **2404:** 355–362. doi:10.1007/978-1-0716-1851-6_19

Cao C, Ma Q, Huang X, Li A, Liu J, Ye J, Gui Y. 2021. Targeted demethylation of the PLOD2 mRNA inhibits the proliferation and migration of renal cell carcinoma. *Front Mol Biosci* **8:** 675683. doi:10.3389/fmolb.2021.675683

Chen L, Gao Y, Xu S, Yuan J, Wang M, Li T, Gong J. 2023. N^6-Methyladenosine reader YTHDF family in biological processes: structures, roles, and mechanisms. *Front Immunol* **14:** 1162607. doi:10.3389/fimmu.2023.1162607

Chen T, Greene GH, Motley J, Mwimba M, Luo GZ, Xu G, Karapetyan S, Xiang Y, Liu C, He C, et al. 2024. m^{6}A modification plays an integral role in mRNA stability and translation during pattern-triggered immunity. *Proc Natl Acad Sci* **121:** e2411100121. doi:10.1073/pnas.2411100121

Cox DBT, Gootenberg JS, Abudayyeh OO, Franklin B, Kellner MJ, Joung J, Zhang F. 2017. RNA editing with CRISPR-Cas13. *Science* **358:** 1019–1027. doi:10.1126/science.aaq0180

Gruber C, Krautner L, Bergant V, Grass V, Ma Z, Rheinemann L, Krus A, Reinhardt F, Mazneykova L, Rocha-Hasler M, et al. 2024. Engineered, nucleocytoplasmic shuttling Cas13d enables highly efficient cytosolic RNA targeting. *Cell Discov* **10:** 42. doi:10.1038/s41421-024-00672-1

Gupta R, Ghosh A, Chakravarti R, Singh R, Ravichandiran V, Swarnakar S, Ghosh D. 2022. Cas13d: a new molecular scissor for transcriptome engineering. *Front Cell Dev Biol* **10:** 866800. doi:10.3389/fcell.2022.866800

He PC, He C. 2021. m^{6}A RNA methylation: from mechanisms to therapeutic potential. *EMBO J* **40:** e105977. doi:10.15252/embj.2020105977

Karagkouni D, Paraskevopoulou MD, Chatzopoulos S, Vlachos IS, Tastsoglou S, Kanellos I, Papadimitriou D, Kavakiotis I, Maniou S, Skoufos G, et al. 2018. DIANA-TarBase v8: a decade-long collection of experimentally supported miRNA-gene interactions. *Nucleic Acids Res* **46:** D239–D245. doi:10.1093/nar/gkx1141

Kennedy MA, Hosford CJ, Azumaya CM, Luyten YA, Chen M, Morgan RD, Stoddard BL. 2023. Structures, activity and mechanism of the type IIS restriction endonuclease PaqCI. *Nucleic Acids Res* **51:** 4467–4487. doi:10.1093/nar/gkad228

Konermann S, Lotfy P, Brideau NJ, Oki J, Shokhirev MN, Hsu PD. 2018. Transcriptome engineering with RNA-targeting type VI-D CRISPR effectors. *Cell* **173:** 665–676.e14. doi:10.1016/j.cell.2018.02.033

Kretschmer J, Rao H, Hackert P, Sloan KE, Höbartner C, Bohnsack MT. 2018. The m^{6}A reader protein YTHDC2 interacts with the small ribosomal subunit and the 5′-3′ exoribonuclease XRN1. *RNA* **24:** 1339–1350. doi:10.1261/rna.064238.117

Leger A, Amaral PP, Pandolfini L, Capitanchik C, Capraro F, Miano V, Migliori V, Toolan-Kerr P, Sideri T, Enright AJ, et al. 2021. RNA modifications detection by comparative nanopore direct RNA sequencing. *Nat Commun* **12:** 7198. doi:10.1038/s41467-021-27393-3

Li H. 2018. Minimap2: pairwise alignment for nucleotide sequences. *Bioinformatics* **34:** 3094–3100. doi:10.1093/bioinformatics/bty191

Li HB, Tong J, Zhu S, Batista PJ, Duffy EE, Zhao J, Bailis W, Cao G, Kroehling L, Chen Y, et al. 2017. m^{6}A mRNA methylation controls T cell homeostasis by targeting the IL-7/STAT5/SOCS pathways. *Nature* **548:** 338–342. doi:10.1038/nature23450

Li J, Chen Z, Chen F, Xie G, Ling Y, Peng Y, Lin Y, Luo N, Chiang CM, Wang H. 2020. Targeted mRNA demethylation using an engineered dCas13b-ALKBH5 fusion protein. *Nucleic Acids Res* **48:** 5684–5694. doi:10.1093/nar/gkaa269

Liu J, Dou X, Chen C, Chen C, Liu C, Xu MM, Zhao S, Shen B, Gao Y, Han D, et al. 2020. N^6-methyladenosine of chromosome-associated regulatory RNA regulates chromatin state and transcription. *Science* **367:** 580–586. doi:10.1126/science.aay6018

Liu H, Zheng J, Liao A. 2022. The regulation and potential roles of m^{6}A modifications in early embryonic development and immune tolerance at the maternal-fetal interface. *Front Immunol* **13:** 988130. doi:10.3389/fimmu.2022.988130

Marillonnet S, Werner S. 2019. Assembly of complex pathways using type IIs restriction enzymes. *Methods Mol Biol* **1927:** 93–109. doi:10.1007/978-1-4939-9142-6_7

McIntyre ABR, Gokhale NS, Cerchietti L, Jaffrey SR, Horner SM, Mason CE. 2020. Limits in the detection of m^{6}A changes using MeRIP/m^{6}A-seq. *Sci Rep* **10:** 6590. doi:10.1038/s41598-020-63355-3

Meyer KD, Jaffrey SR. 2014. The dynamic epitranscriptome: N^6-methyladenosine and gene expression control. *Nat Rev Mol Cell Biol* **15:** 313–326. doi:10.1038/nrm3785

Molinie B, Giallourakis CC. 2017. Genome-wide location analyses of N6-methyladenosine modifications (m^{6}A-seq). *Methods Mol Biol* **1562:** 45–53. doi:10.1007/978-1-4939-6807-7_4

Nachtergaele S, He C. 2017. The emerging biology of RNA post-transcriptional modifications. *RNA Biol* **14:** 156–163. doi:10.1080/15476286.2016.1267096

Nombela P, Miguel-López B, Blanco S. 2021. The role of m^{6}A, m^{5}C and Psi RNA modifications in cancer: novel therapeutic opportunities. *Mol Cancer* **20:** 18. doi:10.1186/s12943-020-01263-w

Pickar-Oliver A, Gersbach CA. 2019. The next generation of CRISPR-Cas technologies and applications. *Nat Rev Mol Cell Biol* **20:** 490–507. doi:10.1038/s41580-019-0131-5

Prjibelski AD, Mikheenko A, Joglekar A, Smetanin A, Jarroux J, Lapidus AL, Tilgner HU. 2023. Accurate isoform discovery with IsoQuant using long reads. *Nat Biotechnol* **41:** 915–918. doi:10.1038/s41587-022-01565-y

Ramesh-Kumar D, Guil S. 2022. The IGF2BP family of RNA binding proteins links epitranscriptomics to cancer. *Semin Cancer Biol* **86:** 18–31. doi:10.1016/j.semcancer.2022.05.009

Ran FA, Hsu PD, Wright J, Agarwala V, Scott DA, Zhang F. 2013. Genome engineering using the CRISPR-Cas9 system. *Nat Protoc* **8:** 2281–2308. doi:10.1038/nprot.2013.143

Rau K, Rösner L, Rentmeister A. 2019. Sequence-specific m^{6}A demethylation in RNA by FTO fused to RCas9. *RNA* **25:** 1311–1323. doi:10.1261/rna.070706.119

Rauch S, He C, Dickinson BC. 2018. Targeted m^{6}A reader proteins to study epitranscriptomic regulation of single RNAs. *J Am Chem Soc* **140:** 11974–11981. doi:10.1021/jacs.8b05012

Roundtree IA, Evans ME, Pan T, He C. 2017. Dynamic RNA modifications in gene expression regulation. *Cell* **169:** 1187–1200. doi:10.1016/j.cell.2017.05.045

Shan T, Liu F, Wen M, Chen Z, Li S, Wang Y, Cheng H, Zhou Y. 2023. m^{6}A modification negatively regulates translation by switching mRNA from polysome to P-body via IGF2BP3. *Mol Cell* **83:** 4494–4508.e6 doi:10.1016/j.molcel.2023.10.040

Shi P, Wu X. 2024. Programmable RNA targeting with CRISPR-Cas13. *RNA Biol* **21:** 575–583. doi:10.1080/15476286.2024.2351657

Stephenson W, Razaghi R, Busan S, Weeks KM, Timp W, Smibert P. 2022. Direct detection of RNA modifications and structure using single-molecule nanopore sequencing. *Cell Genom* **2:** 100097. doi:10.1016/j.xgen.2022.100097

Sun H, Lu B, Zhang Z, Xiao Y, Zhou Z, Xi L, Li Z, Jiang Z, Zhang J, Wang M, et al. 2025. Mild and ultrafast GLORI enables absolute quantification of

m^{6}A methylome from low-input samples. *Nat Methods* **22:** 1226–1236. doi:10.1038/s41592-025-02680-9
Tan X, Zheng C, Zhuang Y, Jin P, Wang F. 2023. The m6A reader PRRC2A is essential for meiosis I completion during spermatogenesis. *Nat Commun* **14:** 1636. doi:10.1038/s41467-023-37252-y
Tang XE, Tan SX, Hoon S, Yeo GW. 2022. Pre-existing adaptive immunity to the RNA-editing enzyme Cas13d in humans. *Nat Med* **28:** 1372–1376. doi:10.1038/s41591-022-01848-6
Tasnim M, Selph TJ, Olcott J, Hill JT. 2023. The type IIS restriction enzyme MmeI can cut across a double-strand break. *Mol Biol Rep* **50:** 5495–5499. doi:10.1007/s11033-023-08375-8
Terns MP. 2018. CRISPR-based technologies: impact of RNA-targeting systems. *Mol Cell* **72:** 404–412. doi:10.1016/j.molcel.2018.09.018
Wang X, Lu Z, Gomez A, Hon GC, Yue Y, Han D, Fu Y, Parisien M, Dai Q, Jia G, et al. 2014. N6-Methyladenosine-dependent regulation of messenger RNA stability. *Nature* **505:** 117–120. doi:10.1038/nature12730
Wang J, Wang J, Gu Q, Ma Y, Yang Y, Zhu J, Zhang Q. 2020. The biological function of m^{6}A demethylase ALKBH5 and its role in human disease. *Cancer Cell Int* **20:** 347. doi:10.1186/s12935-020-01450-1
Wang X, Zhang R, Yang D, Li G, Fan Z, Du H, Wang Z, Liu Y, Lin J, Wu X, et al. 2023. Develop a compact RNA base editor by fusing ADAR with engineered EcCas6e. *Adv Sci (Weinh)* **10:** e2206813. doi:10.1002/advs.202206813
Wessels HH, Méndez-Mancilla A, Guo X, Legut M, Daniloski Z, Sanjana NE. 2020. Massively parallel Cas13 screens reveal principles for guide RNA design. *Nat Biotechnol* **38:** 722–727. doi:10.1038/s41587-020-0456-9
Wilson C, Chen PJ, Miao Z, Liu DR. 2020. Programmable m^{6}A modification of cellular RNAs with a Cas13-directed methyltransferase. *Nat Biotechnol* **38:** 1431–1440. doi:10.1038/s41587-020-0572-6
Xia Z, Tang M, Ma J, Zhang H, Gimple RC, Prager BC, Tang H, Sun C, Liu F, Lin P, et al. 2021. Epitranscriptomic editing of the RNA N6-methyladenosine modification by dCasRx conjugated methyltransferase and demethylase. *Nucleic Acids Res* **49:** 7361–7374. doi:10.1093/nar/gkab517
Xiang Y, Laurent B, Hsu CH, Nachtergaele S, Lu Z, Sheng W, Xu C, Chen H, Ouyang J, Wang S, et al. 2017. RNA m^{6}a methylation regulates the ultraviolet-induced DNA damage response. *Nature* **543:** 573–576. doi:10.1038/nature21671
Xiao Y, Wang Y, Tang Q, Wei L, Zhang X, Jia G. 2018. An elongation- and ligation-based qPCR amplification method for the radiolabeling-free detection of locus-specific N^6-methyladenosine modification. *Angew Chem Int Ed Engl* **57:** 15995–16000. doi:10.1002/anie.201807942
Xiong X, Yi C, Peng J. 2017. Epitranscriptomics: toward a better understanding of RNA modifications. *Genomics Proteomics Bioinformatics* **15:** 147–153. doi:10.1016/j.gpb.2017.03.003
Xu Y, Zhang Y, Luo Y, Qiu G, Lu J, He M, Wang Y. 2023. Novel insights into the METTL3-METTL14 complex in musculoskeletal diseases. *Cell Death Discov* **9:** 170. doi:10.1038/s41420-023-01435-9
Xuan J, Chen L, Chen Z, Pang J, Huang J, Lin J, Zheng L, Li B, Qu L, Yang J. 2024. RMBase v3.0: decode the landscape, mechanisms and functions of RNA modifications. *Nucleic Acids Res* **52:** D273–D284. doi:10.1093/nar/gkad1070
Yang Z, Zhang S, Xiong J, Xia T, Zhu R, Miao M, Li K, Chen W, Zhang L, You Y, et al. 2024. The m^{6}A demethylases FTO and ALKBH5 aggravate the malignant progression of nasopharyngeal carcinoma by coregulating ARHGAP35. *Cell Death Discov* **10:** 43. doi:10.1038/s41420-024-01810-0
Zaccara S, Jaffrey SR. 2020. A unified model for the function of YTHDF proteins in regulating m^{6}A-modified mRNA. *Cell* **181:** 1582–1595.e18. doi:10.1016/j.cell.2020.05.012
Zhang Y, Lu L, Li X. 2022. Detection technologies for RNA modifications. *Exp Mol Med* **54:** 1601–1616. doi:10.1038/s12276-022-00821-0
Zhang T, Zhao F, Li J, Sun X, Zhang X, Wang H, Fan P, Lai L, Li Z, Sui T. 2024. Programmable RNA 5-methylcytosine (m5C) modification of cellular RNAs by dCasRx conjugated methyltransferase and demethylase. *Nucleic Acids Res* **52:** 2776–2791. doi:10.1093/nar/gkae110
Zheng G, Dahl JA, Niu Y, Fedorcsak P, Huang CM, Li CJ, Vågbø CB, Shi Y, Wang WL, Song SH, et al. 2013. ALKBH5 is a mammalian RNA demethylase that impacts RNA metabolism and mouse fertility. *Mol Cell* **49:** 18–29. doi:10.1016/j.molcel.2012.10.015
Zheng P, Zhou C, Ding Y, Liu B, Lu L, Zhu F, Duan S. 2023. Nanopore sequencing technology and its applications. *MedComm (2020)* **4:** e316. doi:10.1002/mco2.316
Zhou J, Wan J, Gao X, Zhang X, Jaffrey SR, Qian SB. 2015. Dynamic m^{6}A mRNA methylation directs translational control of heat shock response. *Nature* **526:** 591–594. doi:10.1038/nature15377
Zhou Z, Lv J, Yu H, Han J, Yang X, Feng D, Wu Q, Yuan B, Lu Q, Yang H. 2020. Mechanism of RNA modification N6-methyladenosine in human cancer. *Mol Cancer* **19:** 104. doi:10.1186/s12943-020-01216-3
Zhu ZM, Huo FC, Zhang J, Shan HJ, Pei DS. 2023. Crosstalk between m6A modification and alternative splicing during cancer progression. *Clin Transl Med* **13:** e1460. doi:10.1002/ctm2.1460

Received January 28, 2025; accepted in revised form October 11, 2025.